ORIGINAL PAPER

Effect of extrusion on the foaming behavior of thermoplastic polyurethane with different hard segments

Shu-Kai Yeh[1] · Raghavendrakumar Rangappa[1] · Ting-Hao Hsu[1] · Stephen Utomo[1]

Abstract

Although it is known that the extrusion process significantly affects the cell morphology of thermoplastic polyurethane (TPU) foam, its effect on foam shrinkage, which is a critical problem in foam processing, has not yet been studied. Extrusion also significantly influences the thermomechanical properties and foaming behavior of TPUs. In this study, polyether-based TPUs of three different hardness levels were foamed by one-step batch foaming using CO_2 as the blowing agent. Although the molecular weight decreased significantly after extrusion, the re-distribution of hard segments in the TPU caused the cell density to increase by 30 to 50 times. In addition, the elongation at break of the TPU solids increased by 40%.

The cell size, expansion ratio, cell density, and shrinkage versus saturation temperature (T_{sat}), and saturation pressure (P_{sat}) were also studied extensively. The results show that T_{sat} has a significant effect on expansion ratio and P_{sat} has more impact on foam shrinkage, while the extrusion processing has little impact on foam shrinkage. In our case, a TPU foam with more than six times expansion and a fine cell structure with limited shrinkage was successfully prepared.

Keywords Carbon dioxide · Elastomer foam · Foam shrinkage · Thermoplastic polyurethane · Bead foam · Hardness

Introduction

In recent years, thermoplastic elastomer (TPE) foams have attracted much interest in both science and industry because of their specific properties such as low density, thermal and acoustic insulation, and good energy absorption capability [1]. Among the TPEs, the use of thermoplastic polyurethane (TPU) foam shows a high growth rate due to the recent growing demand for footwear applications. TPU possesses excellent chemical and abrasion resistance compared to conventional rubber [2], and the price is the lowest among high-performance elastomers [3].

TPUs are composed of soft and hard segments. The soft segment is usually a polyester or polyether polyol, which affects the flexibility, while the hard segment (HS) consists of isocyanate and a chain extender to control the rigidity and mechanical properties. The physical and chemical properties of TPUs and their foam can be manipulated by varying the ratio of soft and hard segments, heat treatments, and processing conditions [4–8].

TPU foams have many applications, such as in the footwear industry and for biomedical and chemical mechanical polishing pads [9–11]. A good example is the expandable TPU (ETPU) bead foam material used in shoe soles, where the performance of TPU foam-based midsoles, compared with conventional ethylene–vinyl acetate foam-based midsoles, is superior in several aspects, for example its high energy absorption capability, wear resistance, toughness, and durability [12]. In the fast-growing footwear industry, foaming TPU has become one of the most active research areas in polymeric foam. A brief review can be found in our previous publication [4].

Hossieny et al. studied the effect of the annealing process on TPU crystallinity and the resultant foam structure using butane as the blowing agent [6, 7]. After extrusion, the HS was rearranged, causing cell density to increase by about two orders of magnitude. Nofar et al. systematically have investigated the effect of different HS contents, SS molecular weight, and processing parameters on the foaming behavior of polyester-based TPU [8, 13]. The increase in HS content led to an increase in hardness, and the foam shrinkage was minimized. Because the increase in HS crystallinity

✉ Shu-Kai Yeh
  skyeh@mail.ntust.edu.tw

[1] Department of Materials Science and Engineering, National Taiwan University of Science and Engineering, Taipei, Taiwan 10608

promoted heterogeneous nucleation, the crystallinity of TPUs was extensively investigated using DSC. The saturation temperature, pressure, and time influenced HS crystal size and crystallinity in TPU. The increase in the SS molecular weight not only helped improve the flexibility of TPUs, it also broadened the HS crystal size distribution. Therefore, the foam processing window widened and the foam shrinkage was significantly reduced. Finally, foaming may destruct HS crystallization. All of these issues may affect the morphology and thus the properties of TPU foam.

In a typical bead foaming process, the polymer pellets are suspended in water inside a high-pressure vessel and are foamed by fast pressure release. The rapid expansion during foaming stretches the molecular chain in the cell wall by biaxial elongation [14]. The diffusion rate of the blowing agent out of the foam needs to be slower than that of air into the foam. Otherwise, the total pressure inside the cells may be lower than the atmospheric pressure, leading to foam shrinkage and surface quality problems [15]. Foaming or cell growth happens above the melting or softening point of the polymer, which is related to non-isothermal extensional rheology [16, 17]. Foam shrinkage happens when materials solidify, which is related to the viscoelastic behavior of the solid polymer. The mechanical properties of the polymers, the diffusivity of the blowing agent, the solubility of the blowing agent in the polymer matrix, and cell wall thickness are critical factors in foam shrinkage [18]. Depending on the type of blowing agent and the viscoelasticity behavior of the polymer, the foam may first expand and then shrink [18] or may shrink immediately and re-expand during the blowing agent/air counter-diffusion process [19, 20].

Low-density polyethylene (LDPE) foam shrinkage problems have been studied extensively. Briscoe and Savvas, who have studied the gas diffusion and foam shrinkage in nitrogen expanded LDPE semifoams [18], simulate the foam shrinkage by assuming that polymeric foams are a series of membrane pistons permeable by gas. By knowing the initial and final size of the foam, they can estimate the volume strain, initial gas pressure in the cells, initial cell volume fraction, spring constant, and viscous constant of the polymer matrix and the shrinkage behavior can be simulated by solving complex mass balance differential equations. Their simulation method shows that the viscoelastic behavior of the polymer significantly affects the foam shrinkage.

Yang et al. used a similar concept to simulate the shrinkage of isobutane-blown LDPE foam. Instead of using the Voigt model, Yang et al. applied the Maxwell model to describe the polymer viscoelasticity [19, 20]. Zhang et al. adopted Yang's approach and studied the shrinkage behavior of LDPE foams and foams made with a mixture of blowing agents [21, 22]. ETPU is usually made of TPU with hardness levels from 62 to 95A [23, 24], which can be converted to a Young's modulus between 4 and 44 MPa [25], a value

that is significantly lower than that of LDPE. Polymers with a low modulus, which is the linear elastic response of the polymer, have a low spring constant and thus much more severe shrinkage.

A typical strategy to enhance the modulus and thus reduce foam shrinkage is to add rigid polymers or nanoparticles. Acrylonitrile butadiene styrene, polytetrafluoroethylene, polylactic acid, and nanoclay have been used for these applications [26–28]; however, they may not be the only choices. Zhao et al. studied the effect of foaming parameters on TPU/water mixtures using the research surface methodology [29]. They found that saturation temperature (T_{sat}) was the most significant factor affecting the shrinkage ratio. Hossieny et al. and Yang et al. proposed that plasticizers such as glycerol monostearate eventually migrate to the surface of the cell to prevent gas loss [6, 20], while Lan et al. have proposed that the dissociation of hydrogen bonds upon heating TPU may play an important role in foam shrinkage [30]. Note that except for Zhao's work [29], the samples in all of these studies were foamed without suspending the TPU in water.

As previously mentioned, extrusion significantly increases cell density. However, to our knowledge, its effect on foam shrinkage has not yet been studied. In this study, we investigate the effect of extrusion and other processing variables on the foaming and shrinkage behaviors of polyether-based TPU using CO_2 as the physical blowing agent. Carbon dioxide was chosen as the blowing agent because it is environmentally friendly and inflammable [31]. The foam was prepared by one-step batch foaming without suspending the TPU in water because water may act as a co-blowing agent and increase the complexity of the analysis [32, 33]. In addition, drying the foamed beads increases energy consumption.

Because the diffusion rate of CO_2 in polymer is significantly higher than that of other common blowing agents such as isobutane [34], CO_2 blown ETPUs are expected to have rapid and apparent foam shrinkage. Understanding the correlations between foam shrinkage and hardness and processing variables will be valuable in understanding the TPU foaming process.

Experimental methods

Materials

Polyether-based TPUs supplied by Kin Join Co., Ltd. were used in this study. The TPUs had material grades of E385, E390, and E395, which represent a hardness of 85A, 90A, and 95A, respectively. The soft segment was poly-tetramethylene ether glycol (PTMEG) with a molecular weight of 1000 g/mol. The HS was 4–4'-methylene

diphenyl diisocyanate (MDI) and 1.4-butanediol (BD). The hard segment contents of the TPU, from soft to hard, were 39.3 wt%, 45.9 wt%, and 50.4 wt%, respectively. Note that no additives or processing aids were added to eliminate the impact of additives during foaming and that before any experiment or process, the TPUs were pre-dried in a vacuum oven at 80 °C for 16 h to remove the moisture. The blowing agent, carbon dioxide (99.99% purity), was purchased from Wanan Gas Co., Ltd.

Sample preparation

Because its processing history may change the molecular structure and foaming ability of TPU [7], we examined the effects of extrusion on its physical properties and cell structure. Approximately five grams of "as-received" TPU materials (AR-TPU) with different hardness levels (85A, 90A, and 95A) were compounded using an Xplore MC-15 micro-compounder in a nitrogen atmosphere with a screw speed and time of 60 rpm and 5 min. An extrusion temperature of 200 °C was selected for 85A and 90A to prevent 85A and 90A TPU from degradation. At a processing temperature of 210 °C, 85A and 90A-TPU samples became yellow. However, the extrusion temperature for 95A was increased to 210 °C to melt the polymer, as at an extrusion temperature of 200 °C, the extrudate of 95A-TPU was turbid, perhaps due to the incomplete melt of HS domain. When the processing temperature increased to 210 °C, the extrudate became transparent and no apparent yellowing was observed. For this reason, a processing temperature of 210 °C was applied for 95A-TPU samples. The extrudate strands were quenched in an ice/water bath and cut into pellet form. These samples are labeled "PR-TPU".

Material characterization

The melt flow index (MFI) tests of the pre-dried TPU were at 190 °C and 10 kg using a Dynisco LMI 5000 melt flow indexer. The hardness of the TPU was determined using a Teclock GS-709G Shore A hardness tester according to ASTM D2240. The TPU pellets were compression-molded into 2 mm thick disks by a hot press and stacked to a thickness of 6 mm for hardness testing. The molecular weight of the TPU samples was determined by advanced polymer chromatography (APC) from Waters ACQUITY using polystyrene standards. A TPU solution with 0.2 wt% concentration was prepared by dissolving 10 mg of the sample in 5 ml of tetrahydrofuran (THF) using an ultrasonicator, with the instrument temperature set to 45 °C and the THF flow rate at 0.8 ml/min.

Mechanical properties measurement

The compounded TPU pellets were injection-molded into ASTM D638 Type V tensile test bars at 200 °C and 45 MPa using a Shinko Sellbic Model 0813 micro injection molding machine. All samples were allowed to settle for at least 48 h before further testing.

The tensile test was performed on a World Metrology TM-2101 Universal tensile machine equipped with pneumatic grips and rubber grip pads to prevent sample slippage. The pressure of the grip was set at 6 kg/cm^2. The test was conducted at a crosshead speed of 100 mm/min at room temperature.

Thermal analysis

Differential scanning calorimetry (DSC)

The HS crystallization behavior of TPU was studied using a TA Instruments Discovery DSC 250 in a heat-cool-heat process with a heating/cooling rate of 10 ºC/min. The samples, which were heated to 230 °C, cooled to –50 °C and heated again to 230 °C, weighed between 5 and 10 mg.

Thermomechanical analysis (TMA)

The softening temperature of the TPU samples was analyzed by thermomechanical analysis (TA Instruments TMA Q400EM). According to ASTM E1545, the softening temperature is defined by extrapolating the data points at which the displacement abruptly changes. The TPU pellets were compression-molded into a 2 mm thick film and analyzed with a penetrating probe from room temperature to 180 °C with a heating rate of 5 °C/min and an applied force of 50 mN. The test was conducted in a nitrogen atmosphere.

Foaming

The TPU strands were cut into pellets of approximately 0.05 g and used for foaming. The experiments were conducted at various T_{sat} using CO_2 as the blowing agent. The schematic diagram of the foaming system (see Fig. S1) shows that the foaming vessels (Swagelok SS-2F-05) are connected to a syringe pump (ISCO-265D) via a four-way union. Each vessel was connected to a three-way ball valve for pressure release. The TPU pellet was saturated in the foaming vessel at the desired pressure and temperature for one hour, then foamed by quickly opening the three-way ball valve. T_{sat} ranged from 120 ºC to 150 ºC and the saturation pressure (P_{sat}) varied from 5.52 MPa (800 psi) to 13.79 MPa (2000 psi) with intervals of 2.07 MPa (300 psi). After pressure release, the vessels were quenched in an ice/water bath to freeze the cell structure. The saturation time one hour

was selected based on our previous study [35]. We carefully compared the cell structure of synthesized TPU saturated for 1 h and 24 h. The cell structure of the various synthesized foams did not change with saturation time.

The cell morphology of the foamed sample was observed using JEOL JSM-6390LV SEM. After foaming, the samples were left at atmospheric pressure and 25 °C for five days to stabilize the cell structure. Then samples were cryo-fractured in liquid nitrogen and coated with platinum before observation.

Foam density, foam expansion, and shrinkage ratio

Density was determined by the Archimedes principle based on ASTM D792. The shrinkage ratio (S) of the foams was also calculated using the expansion ratio results from Eq. (1), where ϕ_i is the expansion ratio of samples foamed after 1 h and S(t) is the expansion ratio at time t. The elastic nature of TPU and the high diffusivity of CO_2 caused the sample to shrink quickly. In addition, after pressure release, the foamed samples were immediately quenched in an ice/water bath. This quenching might further reduce the gas pressure inside the cell and increase the pressure difference between the inside and outside of the foam. For polymers such as TPU, the compressive moduli are low. Thus, the increase in pressure difference may lead to even more severe foam shrinkage. In a typical example, as shown in Fig. S2, the TPU foamed at 13.79 MPa shrank significantly within 3 min. All of these issues made it very difficult to determine the initial foam expansion ratio. Although Lan et al. [30, 36] and Wang et al. [27] mentioned the shrinkage ratio in their work, they did not explain how the expansion ratio at time zero ($\phi(0)$) was determined. In this study, we chose the expansion ratio at one hour after foaming and define it as ϕ_i and the final expansion ratio (ϕ_f), defined as ($\phi(120\,h)$).

$$S(t) = \frac{\phi_i - \phi(t)}{\phi_i} \times 100 \qquad (1)$$

Cell analysis

Cell size was calculated from the SEM images with more than 100 cells using SG View software. The cell density was calculated by Eq. (2) [37].

$$N_f = \left(\frac{nM^2}{A}\right)^{\frac{3}{2}} \left(\frac{\rho_s}{\rho_f}\right) \qquad (2)$$

where N_f is cell density (cells/cm^3), M is SEM picture magnification, n is the number of cells in the SEM picture (cells), and A is the cross-section area of the SEM picture (cm^2). If

we assume the cell was spherical, the cell wall thickness can be determined by Eq. (3) [38].

$$t = L \times \left[\left(1 - \frac{\rho_f}{\rho_s} \right)^{-\frac{1}{3}} - 1 \right] \qquad (3)$$

where ρ_s is the solid polymer density, ρ_f is the foam density, L is average cell diameter, and t is the average cell wall thickness.

Results and discussion

Effect of extrusion on physical properties of TPU at different hardness levels

According to Hossieny et al. the HS distribution may significantly affect the foaming behavior of TPU [7]. Extrusion or mixing may rearrange the HSs so that the segments are evenly dispersed in the matrix, significantly improving the cell structure. In this section, the morphology of TPU foams prepared with AR-TPU and PR-TPU are compared.

The viscosity of TPU during extrusion was monitored by data acquisition software. Despite the differences in hardness and processing temperature, the viscosity of TPU decreased by 43 ~ 45% during extrusion, as shown in Fig. S3. Note that the extrusion was done in a nitrogen atmosphere to prevent TPU oxidation. The decrease in viscosity could be the result of thermal and mechanical degradation.

The APC results, shown in Table S1, reveal that when compounded, the molecular weight (M_w) of the TPU samples, decreased by 31.3%, 35.7%, and 38.3% for 85A-TPU, 90A-TPU, and 95A-TPU, respectively. The polydispersity index (PDI) also decreased after extrusion, indicating that extrusion narrowed the molecular weight distribution.

Hayashi et al. showed that if the MFI value of the TPU sample at 190 °C/10 kg is higher than 40 g/10 min, the foam may have remarkable shrinkage [39]. Thus, the MFI of the AR-TPU and PR-TPU samples was measured to clarify the effect of extrusion on the viscosity, as shown in Table S2: after extrusion, the MFI increased to more than 40 g/10 min. The foaming ability of the PR-TPUs is discussed in Sect. 3.2.

Mechanical properties

The mechanical properties and hardness of TPUs before and after processing are listed in Table 1, and the typical stress–strain curve of the samples is shown in Fig. S4. The results reveal that the hardness and modulus of TPU were not affected by extrusion, but that strength and elongation at break were.

Kojio et al. and Furukawa et al. who explored the relationship between phase separation and mechanical

Table 1 Tensile properties of AR-TPU and PR-TPU

Sample	Young's modulus (MPa)	Maximum strength (MPa)	Elongation at break (%)	Hardness (Shore A)
85A-AR	28.61 ± 1.55	15.43 ± 0.62	301.7 ± 23.0	84
85A-PR	25.94 ± 0.10	24.64 ± 0.72	668.0 ± 14.9	83
90A-AR	33.58 ± 2.10	27.69 ± 0.69	406.7 ± 39.2	89
90A-PR	34.12 ± 0.28	26.64 ± 1.57	581.5 ± 38.5	87
95A-AR	43.03 ± 1.01	26.51 ± 0.95	405.2 ± 36.1	94
95A-PR	41.14 ± 3.72	35.23 ± 0.94	689.1 ± 11.0	92

properties with TPUs of different hardness level [40, 41], observed that increasing the hard segment content increased both hardness and Young's modulus. Our observations are consistent with those of Furukawa et al. [40]. Note that the elongation at break increased significantly, by at least 40% after processing, which may be the effect of micro-phase separation and hydrogen bonding. Kong et al. investigated the microphase separation of MDI/PTMEG based TPU and found that the elongation at break of TPU increased 50% after annealing [42]. In their case, annealing at 30, 80, 120 and 160 °C for 40 min did not change the degree of microphase separation; however, they believe the HSs were rearranged during annealing, which may have decreased the effective physical crosslinking density, and thus significantly increased the elongation at break of the TPU. A similar phenomenon may have happened in our study. Finally, the hardness of TPU decreased slightly after extrusion.

Softening point

The softening temperature (T_s), defined according to ASTM E1545, is the index to determine the saturation/foaming temperature. In the one-step foaming method, the sample should be saturated and foamed between ($T_s - 25$) °C and ($T_s - 10$) °C [43]. The TMA results for AR-TPU and PR-TPU listed in Table 2, 151~162 °C, show that extrusion caused the softening points to drop by 4–10 °C. Note that the drop in T_s increases with the TPU hardness, which could be a result of the decrease in M_w. Using TMA, Keinath and Boyer measured liquid–liquid transition temperature (T_{ll}) of polystyrene, where the definition of T_{ll} is similar to that of T_s [44]. Their results showed that T_{ll} started to decrease as molecular weight below $10^{5.8}$ or 600,000 g/mole. In addition, the greater the drop in M_w, the greater the reduction in T_s. We suspect that similar results may also be observed in TPU, although in our case, the molecular weight of TPU is much less than 600,000 g/mole. Extrusion causes a decrease in molecular weight, and the T_s will decrease accordingly.

Differential scanning calorimeter (DSC) thermal analysis

The production of TPU bead foams requires saturating the materials at elevated temperature and pressure. The saturation process may anneal the molecules and affect the HS crystalline domains; in addition, differences in crystal size or structure may affect foaming behavior, including cell nucleation, foam expansion, and shrinkage.

The DSC curves of TPUs before and after extrusion are shown in Fig. 1 and Table 2. Changes in the structure of the TPU from extrusion can be seen in Fig. 1a. All samples showed two endothermic peaks during the first heating process, one between 100~110 °C and the other between 165~190 °C. The DSC curve may have up to five transitions: the glass transition points (T_g) of the soft segments and the HSs, the short-range order (T_{m1}), the long-range order (T_{m2}), and the melting (T_{m3}) of HS crystals, respectively. The ranges of T_{m1}, T_{m2}, and T_{m3} are 35–115 °C, 130~190 °C, and above 200 °C, respectively [45–47]. The short-range order and the long-range order are both related to hydrogen bonding: the short-range order is associate with urethane-macroglycol bonding while the long-range order is associated with urethane-urethane bonding [45]. The soft segment T_g is generally between –50 and –10 °C depending on the degree of microphase separation [47], and
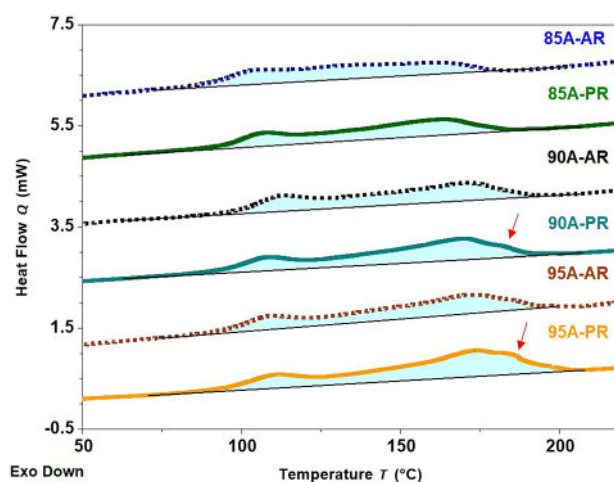

Fig. 1 The first heating DSC curves of AR-TPU and PR-TPU

Table 2 Thermal properties of AR-TPU and PR-TPU with different hardness levels

Material		T_s (°C)	T_g (°C)	T_{m1} (°C)	$T_{m2\text{-low}}$ (°C)	$T_{m2\text{-high}}$ (°C)	$\Delta H_{m,\,1st}$ (J/g)
85A	AR	161.7	−35.0	103.6	165.3	-	18.75
	PR	154.0	−38.6	106.3	163.3	-	23.29
90A	AR	166.6	−30.0	111.9	170.0	-	25.85
	PR	163.3	−34.5	107.0	169.1	182.8	30.00
95A	AR	170.7	−32.4	108.3	170.8	-	24.50
	PR	165.3	−38.2	110.5	173.3	185.0	30.76

the T_g of the MDI/BD HS is 108 °C [48]. Although the soft segment T_g is not shown in Fig. 1, it was around –30~–39 °C, as reported in Table 2.

Based on the definition, the two peaks in the DSC diagram may not be the melting points of the MDI/BD crystals; they could be the short-range order T_{m1} and the long-range order T_{m2}, or the low temperature peak could be the HS T_g. However, since there is no low temperature peak at the second heat scan, as can be seen in Fig. S5, we believe that the low temperature peak is the short-range order, T_{m1}, and the high-temperature peak is the long-range order, T_{m2}. No HS crystal melting peak was observed in our samples.

Although Abouzahr et al. showed that some crystallization occurs at HS content higher than 45 wt% in PTMEG-MDI-BD based TPU systems [49], their crystal structure was determined by a wide-angle X-ray scattering technique, not DSC. Since the highest HS content in our TPU is 50 wt%, such a difference may not be revealed in DSC.

Extrusion changed not only the mechanical properties of TPU, it also changed the melting behavior. In general, extrusion causes a decrease in the M_w of TPUs, which results in lower viscosity, and the shortened molecular chain may easily form an ordered structure. As can be seen in Table 2, the total area under both peaks, ΔH_m, increased after post processing. In addition, the short-range order temperature, T_{m1}, generally increased with the hard segment content.

However, extrusion did not significantly alter T_{m1} or the long-range order peak temperature, $T_{m2\text{-low}}$. With the increase of the hard segment content, a shoulder peak within the long-range order peak, denoted $T_{m2\text{-high}}$, was observed in 90A-PR and 95A-PR samples. Similar results were demonstrated by Hosseiny et al. [6]. Since extrusion thoroughly mixed the HS, the HS was re-ordered and formed an endothermic peak in the range of 182 °C ~ 185 °C during heating.

Effect of extrusion and foaming temperature on the foaming behavior

The significant increase in ΔH_m from extrusion may significantly change the cell morphology [7]. An increase in ΔH_m implies more ordered structures in the TPU, which could act as nucleating sites and result in a much higher cell density. By controlling the HS domains, we may be able to control the cell morphology, expansion ratio, and even shrinkage behavior of the TPU foams. In this section, the effect of extrusion on the foam structure is investigated.

The AR and PR-TPUs were saturated at 7.58 MPa (1100 psi) with various T_{sat} for 1 h and foamed and the ϕ_f is shown in Fig. 2. As can be seen from Fig. 2, extrusion lowered the peak expansion temperature (T_{peak}) by 10–20 °C, consistent with the decrease in T_s, as can be seen in Table 2. Also, extrusion only slightly changed the maximum expansion ratio of the 85A and 90A samples, but after extrusion, the maximum expansion ratio of 95A TPU samples decreased from 6.6 times to 3 times. The difference in expansion ratio may be explained by observing the microstructure of the foam, as shown in Fig. 3. Extrusion increased the cell density and decreased the cell size significantly. Figure 4 shows the HS crystal distribution after extrusion.

However, with or without extrusion, 90A and 95A samples showed big voids or cleavages in the bead, while 85A samples showed a homogeneous cellular structure. As rapid pressure relief of the gas caused cracks in elastomers, the big
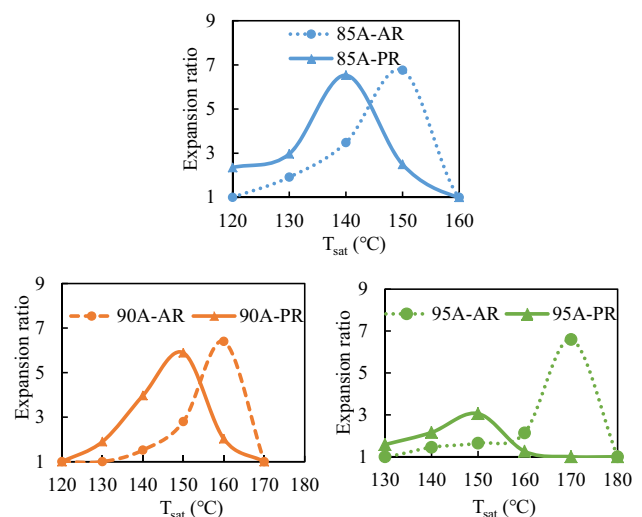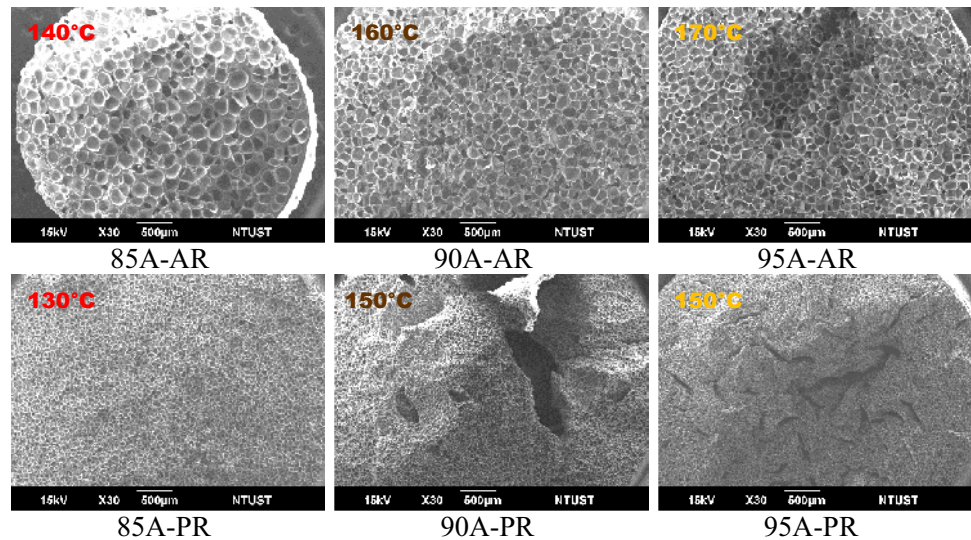

Fig. 2 Final expansion ratio of TPU-AR and PR foamed at different T_{sat} (°C)

Fig. 3 The cell morphologies of the TPU-AR and PR foams at T_{peak} under P_{sat} of 7.58 MPa at various T_{sat}

voids and cleavages in the 95A AR and 90A PR foam may contribute significantly to the expansion ratio. In a detailed review of the origin of pneumatic stress-induced ruptures in elastomers, Briscoe et al. [50] concluded that fast depressurization causes triaxial stresses and a gas concentration gradient inside the polymer which may result cracks. Crack formation is undoubtedly a complex problem. We believe that it may be related to the short-range and long-range order structures of the HS domain in the TPUs.

Briscoe et al.'s review also indicated that high P_{sat} may be undesirable. As previously mentioned, extrusion increased ΔH_m and the amount of HS ordered structure in the polymers, as did saturating the polymer under high pressure CO_2. The higher the hardness, the more the ΔH_m increased [8]. We think that a large number of the HS-ordered structures in the TPU may act as both nucleation sites and stress

concentration points. The rapid expansion of the TPU during foaming tends to stretch the molecular chains of TPU, which led to internal stresses between the amorphous phase and the ordered structure in the TPU and caused the cracks during foaming [51]. Under any circumstances, large cracks in materials are undesirable.

The SEM images in Fig. S6, taken in an area free of voids or cracks illustrate the microstructure of TPUs before and after extrusion. The cell size and cell density were plotted against T_{sat} to identify the effect of temperature on the cell structure at different hardness levels. The temperatures, from $T_{peak} - 20$ °C to T_{peak}, were chosen because most of the cells collapsed above T_{peak}. The cell size and cell density in these SEM images, as shown in Fig. 5, demonstrate that the extrusion significantly increased the cell density and decreased the cell size. On
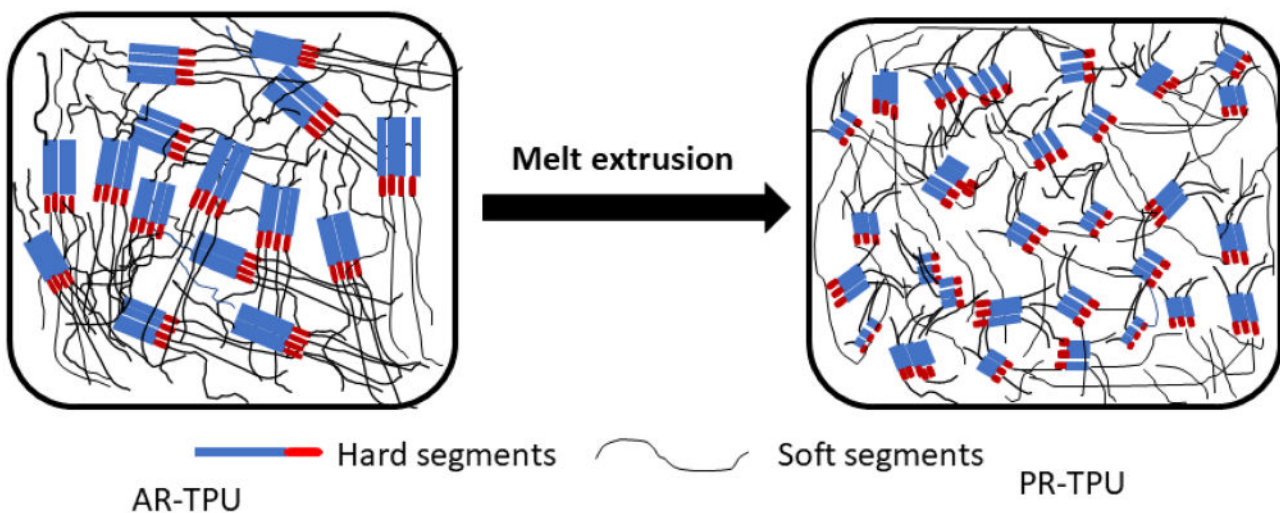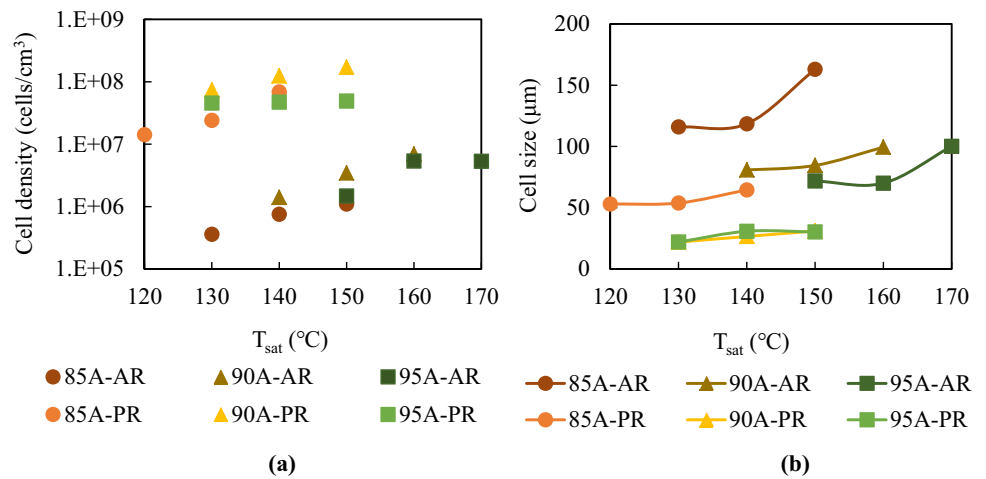

Fig. 4 HS crystal distribution after extrusion

Fig. 5 (a) Cell density, (b) Cell size of TPU-AR and PR at different T_{sat} (℃)

● 85A-AR   ▲ 90A-AR   ■ 95A-AR
● 85A-PR   ▲ 90A-PR   ■ 95A-PR

(a)

● 85A-AR   ▲ 90A-AR   ■ 95A-AR
● 85A-PR   ▲ 90A-PR   ■ 95A-PR

(b)

the other hand, temperature had less impact on cell size or density than extrusion. Increasing T_{sat} may reduce the viscosity of the polymer, and the cell size usually increases in the one-step foaming process [52], but because the cell size was also affected by the severity of the foam shrinkage and cell density, similar phenomena were not observed.

According to classical nucleation theory, the cell density should be proportional to the inverse of the temperature; however, our observations are not in line with the theory. In this study, the TPU at higher hardness levels has more HSs. Also, the TPU was annealed during saturation and the ΔH_m of the long range order increased with T_{sat} [7]. Therefore, increasing both hardness and T_{sat} increased the potential nucleation sites in the TPU, and this increase was responsible for the increase in cell density. As previously mentioned, extrusion did not change the peak expansion ratio. The decrease in cell size, from well above 50 µm to 40 ~ 65 µm after extrusion, compensate for the increase in cell density. Cell size or cell density might not affect the moduli of foams of similar relative density, but a fine cell structure is desirable for increasing fracture toughness and improving the fatigue life of the foam [53–55].

Because large voids or cleavages are defects, neither 90A-TPU nor 95A-TPU can be considered a quality foam product. Therefore, 85A-PR TPU was used to pursue the effect of processing parameters on the foaming. Note that although the MFI of our PR sample was higher than 40 g/10 min, our results show that the maximum shrinkage ratio did not change significantly [39].

Effect of P_{sat} on foaming behavior of TPU

In addition to T_{sat}, P_{sat} is considered a factor that controls cell size and cell density [56]. Because P_{sat} is directly related to the initial pressure in the cell, it affects not only the cell morphology, but also the foam shrinkage. The ϕ_i and ϕ_f of 85A-PR TPU foamed between 120 ~ 150 °C with P_{sat} of 7.58 and 13.79 MPa, as shown in Fig. 6, illustrate the effect of P_{sat}. Foaming at 13.79 MPa may provide a slightly higher ϕ_i but also more severe shrinkage. In addition, we found that the T_{peak} of 85A-PR dropped to 130 °C at a P_{sat} of 13.79 MPa, which may have been caused by the increased CO_2 solubility [57].

To examine the influence of P_{sat} on TPU foaming behavior, 85A-PR TPU was saturated at 140 °C (T_{peak}) with

Fig. 6 85A-PR TPU foamed between 120 ~ 150 °C with P_{sat} of (**a**) 13.79 MPa and (**b**) 7.58 MPa
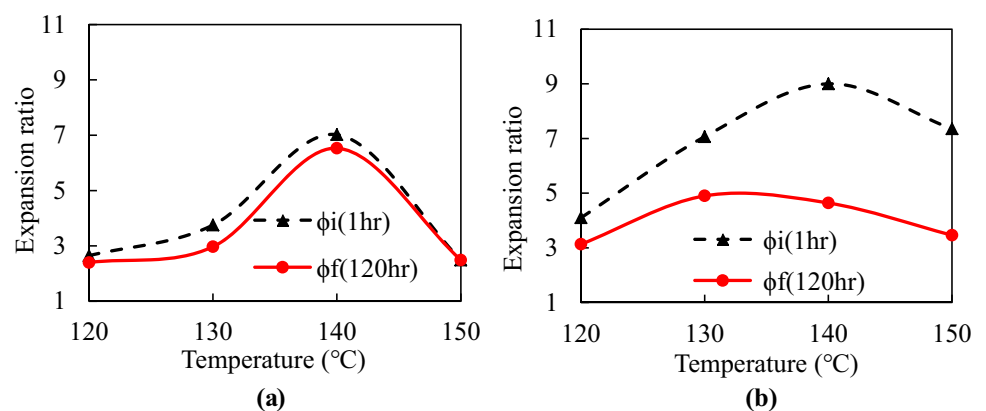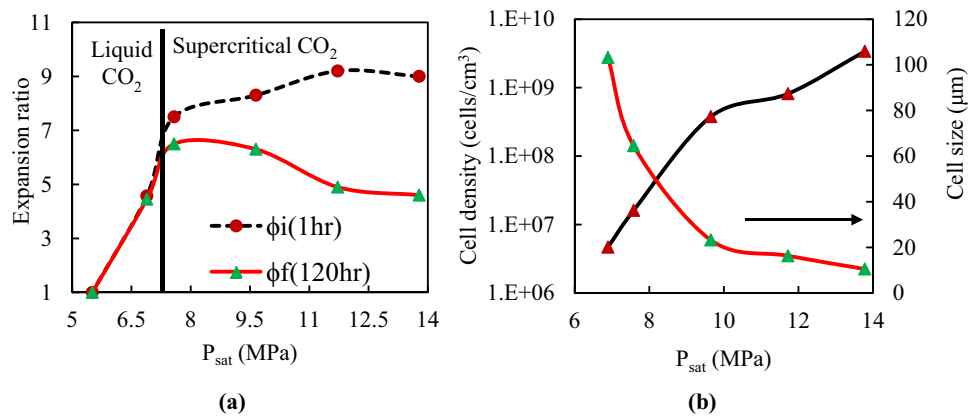

(a)

(b)

Fig. 7 (**a**) Expansion ratio (**b**) Cell density and cell size of the 85A-PR TPU foamed samples saturated at T_{sat} of 140 °C for 1 h at different P_{sat}

(a)

(b)

different degrees of P_{sat} for 1 h and then foamed. The ϕ_i and ϕ_f versus P_{sat} and the cell size and density versus P_{sat}, as shown in Fig. 7, reveal the impact of P_{sat} on the expansion ratio and cell morphology. As can be seen in Fig. 7a, ϕ_i increased with P_{sat} and then leveled off, which is an interesting observation. Also, the ϕ_i did not change significantly above 7.38 MPa, which is the critical pressure for CO_2.

Using TPU foams prepared at P_{sat} higher than 7.58 MPa resulted in a fine cell structure and a high cell density, as shown in Fig. 7b, results that are consistent with our previous study [56] and can be explained by classical nucleation theory. The cell size of commercial ETPU is 50~300 μm [24], and foaming TPU at 7.58 MPa satisfied the cell size criterion.

Figure 8a–d shows beads of 85A-PR TPU foamed at 140 °C under various P_{sat}, with the P_{sat} and shrinkage ratios at the bottom of each figure. As can be seen in Fig. 8, increasing P_{sat} resulted in severe foam shrinkage. At a P_{sat} of 13.79 MPa, the shrinkage ratio reached 48.8%, and the foam appearance was not acceptable. As P_{sat} decreased to 7.58 MPa, the shrinkage ratio decreased to 12.7%, the ϕ_f was the highest (6.5 times) and the foam appearance was acceptable.

According to Li et al. the solubility of CO_2 in polyether/MDI/BD-based TPU increased linearly with pressure, and the CO_2 solubility doubled when P_{sat} increased from 7.58 MPa to 13.78 MPa [58]. If all of the blowing agents were used for foaming, the expansion ratio should have doubled; however, the ϕ_i difference between the two samples was about 18%, implying that a significant amount of CO_2 was not used for foaming and diffused out of the sample. Considering that the ϕ_i between the two samples are not very different, even though CO_2 may diffuse out of the sample, the sample that was foamed at 13.78 MPa should have a much higher CO_2 concentration inside the cells. In addition, as shown in Fig. 9a, cell wall thickness decreased significantly and then leveled off as P_{sat} equaled 9.65 MPa. A high P_{sat} not only creates a high CO_2 concentration gradient inside and outside the foam but also significantly decreases

the cell wall thickness, which leads to a high CO_2 diffusion rate out of the foam and results in more severe foam shrinkage. Therefore, foaming TPU at 13.78 MPa resulted in the highest shrinkage ratio. The proposed scenario is illustrated in Fig. 9b.

Foam shrinkage dynamics

The severe shrinkage, as can be seen from Fig. S2, makes estimating the initial expansion ratio in this study extremely challenging because foam shrinkage cannot be simulated without knowing the initial expansion ratio [18]. Therefore, when investigating shrinkage behavior, we report only the expansion and shrinkage ratios measured at different time intervals.
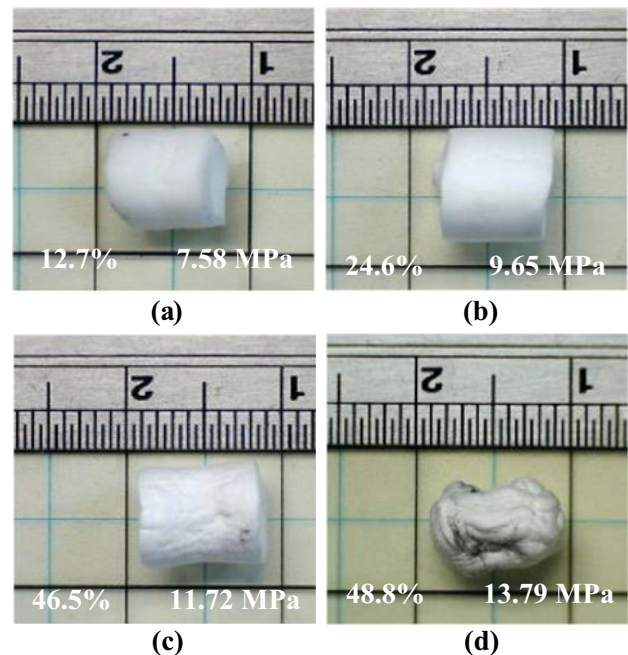

Fig. 8 The appearance of 85A-PR TPU foamed at various P_{sat} and settled in the ambient pressure for 120 h
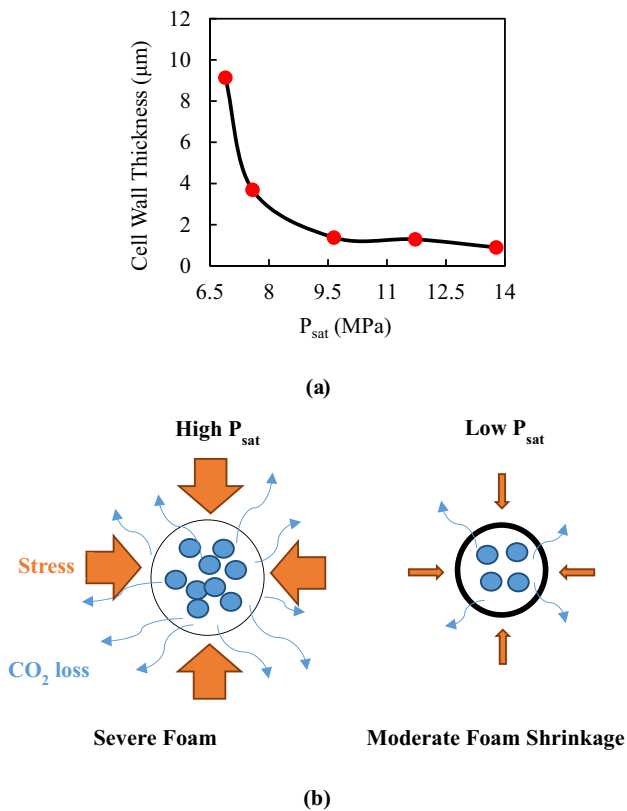
(a)

(b)

Fig. 9 (**a**) Cell wall thickness of 85A -PR TPU foamed samples at a T_{sat} of 140 °C for 1 h under different P_{sat} and (**b**) Schematic diagram of foam shrinkage during high and low-pressure saturation

Effect of processing parameters on shrinkage behavior of foams

Extrusion affects the mechanical and thermal properties of TPUs as well as the foam shrinkage dynamics. The foam expansion ratio versus time, as shown in Fig. 10, demonstrates that the 85A-AR and PR foamed at different T_{sat}. Again, the T_{sat}s were chosen from $T_{peak} - 20$ °C to T_{peak}. The appearance of the foams at 1, 5, and 24 h is shown in Fig. S7. Since CO_2 diffused out of the cells quickly and resulted in severe foam shrinkage, the shrinkage may be caused by a combination of compressive stress resulting from atmospheric pressure and the viscoelastic response of the polymer cell wall. The foam shrinkage behavior is similar to that in Yang's work [19].

As can be seen in Fig. 10a, the T_{sat} apparently affected both the expansion ratio and the shrinkage behavior: samples with a high expansion ratio demonstrated significant foam shrinkage. As discussed previously, cell size was not a strong function of T_{sat}. Therefore, a high expansion ratio can translate into a thin cell wall, as can be seen from Eq. (3). The results confirm that the lower the expansion ratio, the less the foam shrank. Note that because the foam expansion ratio recording started at a time equal to 1 h, the sample that

was foamed at 150 °C shows apparent foam expansion but not foam shrinkage, which can be seen in Fig. S7a. As we mentioned previously, depending on the blowing agent and polymer, the foam may either expand-shrink [18] or shrink-re-expand [19, 20] after foaming. In our case, we only saw foam expansion after one hour. These results imply that the TPU 85A AR foam reached the lowest expansion ratio within one hour when T_{sat} was 150 °C. In addition, in the very beginning, the cells were filled with CO_2 at a pressure higher than 1 atm. After a period of time, the CO_2 concentration inside and outside the cell reached equilibrium. Because the concentration of CO_2 in the atmosphere was low, most of the CO_2 in the cell diffused out of the foam. Even if air were to replace the CO_2 in the cell by diffusion, the final expansion ratio should be less than $\phi(0)$. The $\phi(0)$ of 85 the AR sample foamed at 150 °C should be higher than ϕ_f (6.76 times) [19].

The 85A PR samples foamed at various temperatures are shown in Fig. 10b; the appearance of the foams can be seen in Fig. S7b. After processing, the cell density of the 85A PR samples was 30–50 times higher than that of the 85A AR samples. At a similar expansion ratio, high cell density implies a small cell size and a thin cell wall. Therefore, the 85A PR samples were expected to shrink faster than the 85A AR samples [19]. However, it was not the case. After processing, the elongation at break increased significantly, which implies a decrease in the viscous component of the polymer matrix [59]. Such a decrease could slow the rate of shrinkage. Also, although it cannot be determined easily, the difference in $\phi(0)$ may play an important role as well [19]. In short, the argument that an increase in cell density may slow the foam shrinkage is arbitrary [30]: many other factors affect foam shrinkage.

The shrinkage behavior of the 85A-PR samples foamed at 13.78 MPa and T_{sat} between 120–140 °C are shown in Fig. 10c. Interestingly, although ϕ_i increased with T_{sat}, T_{sat} is not the major factor in the ϕ_f. Samples foamed at 130 °C possessed a higher ϕ_f than those foamed at 140 °C. Again, the high expansion ratio may imply a thin cell wall and thus faster foam shrinkage. The severity of foam shrinkage can be seen in Fig. S7c. At a T_{peak} of 140 °C, a high foaming pressure caused a high ϕ_i. Because the cell wall was stretched well above the elastic limit, the foam collapsed and could not re-expand. The foam shrinkage behavior can be explained using the schematic diagram in Fig. 9b. Carbon dioxide exited the cells easily and created more severe shrinkage. Such phenomena, as discussed previously, may cause a corrugated surface, which is undesirable.

Although cracks were found in the 90A and 95A samples, the foam shrinkage behavior of these samples foamed at 7.58 MPa and their respective T_{peak} were recorded and the results are shown in Fig. S8. Since the moduli of elastomers generally increases with the hardness, even though there were cracks inside the beads, these samples showed less foam shrinkage.

Fig. 10 Shrinkage curves of 85A-AR and PR under different T_{sat} at (**a**, **b**) $P_{sat}=7.58$ MPa and (**c**) 13.78 MPa
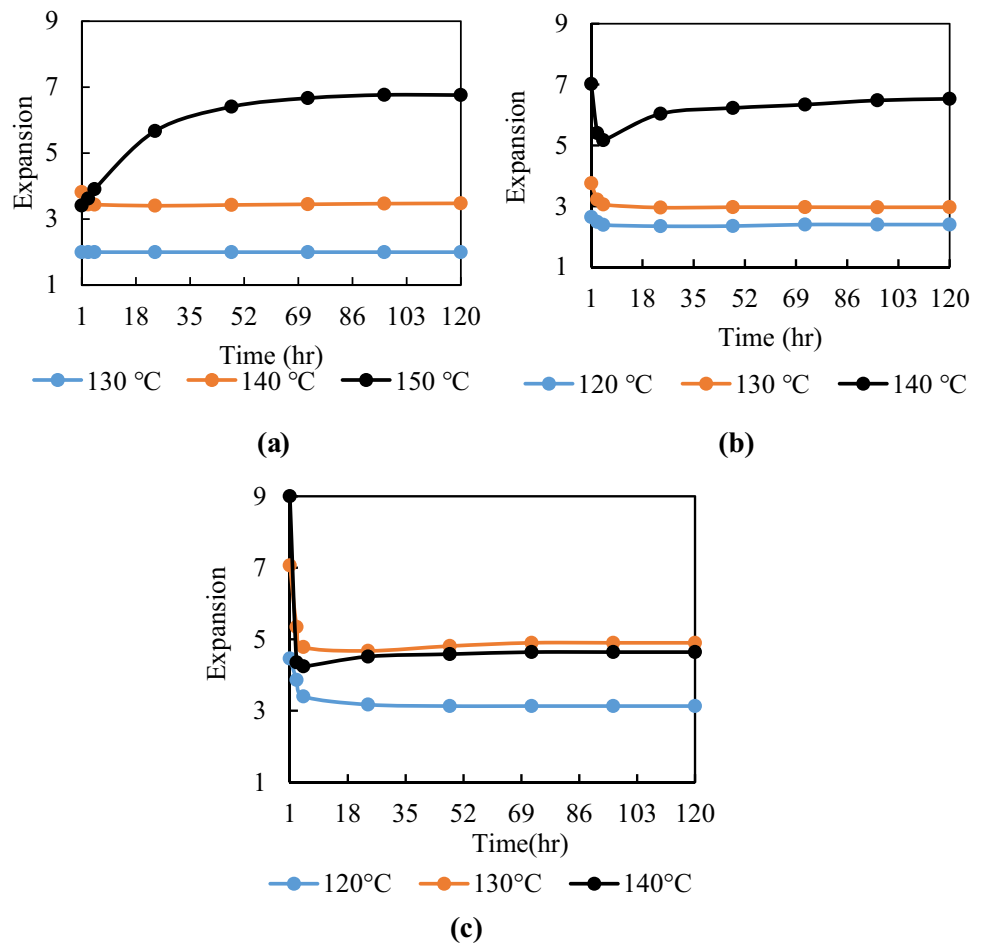
Conclusion

In this study, the effect of extrusion, P_{sat}, and T_{sat} on the cell morphology and expansion ratio of CO_2-blown TPU foam was studied using the MDI/BD/PTMEG TPU as the modelling system. The hardness of the TPU was controlled by varying the hard-segment content. Surprisingly, extrusion increased the elongation at break of the TPU by at least 40% and may have rearranged the HSs. Although the rearrangement in HSs did not create HS crystals in the TPU, it had a significant impact on the cell morphology, and the cell density of the foam increased significantly. The rearrangement in HSs may also have produced stress concentration points and created cracks during the foaming process. Due to the decrease in molecular weight, extrusion caused a $10 \sim 20$ °C decrease in T_s and T_{peak}. The MFI of most of the TPU samples increased to above 40 g/10 min after processing, but the increase in MFI did not cause significant foam shrinkage. In addition, the cell density increased by 30–50 times.

Since the foam shrank so rapidly that $\phi(0)$ cannot be determined, it was not possible to simulate the shrinkage.

However, the foam shrinkage behavior has been extensively discussed. When the sample was foamed at T_{peak}, the thin cell wall caused the expansion ratio of the foam to change significantly over time. On the other hand, the expansion ratio of the foam did not change much at a lower foaming temperature. Because P_{sat} is one of the critical variables in controlling foam shrinkage, foaming at a P_{sat} much higher than CO_2's critical pressure may produce more severe foam shrinkage. The results can be explained using Fig. 9b. Foaming at an elevated P_{sat} should therefore be avoided. Extrusion may slightly delay the foam shrinkage rate but has little impact on the ϕ_f. In summary, by selecting appropriate processing variables and by extrusion, TPU bead foams with a high expansion ratio (6.5 times), fine cell structure (65 μm), and limited foam shrinkage can be obtained.

References

1. Paridokht M, Rodrigue D (2014) Thermoplastic elastomer foams based on recycled rubber. Cell Polym 33:233–248

2. Prisacariu C (2011) Polyurethane elastomers from morphology to mechanical aspects. Springer, New York

3. Kear KE, (2003) Developments in thermoplastic elastomers. Rapra Technology. Shawbury, Shrewsbury, Shropshire, UK

4. Yeh SK, Chen YR, Kang TW, Tseng TJ, Peng SP, Chu CC, Rwei SP, Guo WJ (2018) Different approaches for creating nanocellular TPU foams by supercritical CO_2 foaming. J Polym Res 25:30

5. Chu CC, Yeh SK, Peng SP, Kang TW, Guo WJ, Yang J (2017) Preparation of microporous thermoplastic polyurethane by low-temperature supercritical CO_2 foaming. J Cell Plast 53:135–150

6. Hossieny N, Shaayegan V, Ameli A, Saniei M, Park CB (2017) Characterization of hard-segment crystalline phase of thermoplastic polyurethane in the presence of butane and glycerol monosterate and its impact on mechanical property and microcellular morphology. Polymer 112:208–218

7. Hossieny NJ, Barzegari MR, Nofar M, Mahmood SH, Park CB (2014) Crystallization of hard segment domains with the presence of butane for microcellular thermoplastic polyurethane foams. Polymer 55:651–662

8. Nofar M, Büşra Küçük E, Batı B, (2019) Effect of hard segment content on the microcellular foaming behavior of TPU using supercritical CO_2. J Supercrit Fluids 153:104590

9. Haugen H, Will J, Fuchs W, Wintermantel E, (2006) A novel processing method for injection-molded polyether-urethane scaffolds. part 1: Processing J Biomed Mater Res Part B Appl Biomater 77:65–72

10. Prasad A, Fotou G, Li S (2013) The effect of polymer hardness, pore size, and porosity on the performance of thermoplastic polyurethane-based chemical mechanical polishing pads. J Mater Res 28:2380–2393

11. Ge C, Wang S, Zheng W, Zhai W (2018) Preparation of microcellular thermoplastic polyurethane (TPU) foam and its tensile property. Polym Eng Sci 58:E158–E166

12. Ramirez BJ, Gupta V (2019) Energy absorption and low velocity impact response of open-cell polyurea foams. J Dyn Behav Mater 5:132–142

13. Nofar M, Batı B, Küçük EB, Jalali A, (2020) Effect of soft segment molecular weight on the microcellular foaming behavior of TPU using supercritical CO_2. J Supercrit Fluids 160:104816

14. Keshtkar M, Nofar M, Park CB, Carreau PJ (2014) Extruded PLA/clay nanocomposite foams blown with supercritical CO_2. Polymer 55:4077–4090

15. Eaves D, (2004) Handbook of polymer foams. Rapra Technology, Shawbury, Shrewsbury, Shropshire, UK

16. Koopmans RJ, den Doelder JCF, Paquet AN (2000) Modeling foam growth in thermoplastics. Adv Mater 12:1873–1880

17. den Doelder JCF, Sammler RL, Koopmans RJ, Paquet AN (2002) Modeling foam growth in semi-crystalline thermoplastics. Cell Polym 21:99–116

18. Briscoe BJ, Savvas T (1998) Gas diffusion in dense poly(ethylene) foams. Adv Polym Technol 17:87–106

19. Yang CT, Lee KL, Lee ST (2002) Dimensional stability of LDPE foams: modeling and experiments. J Cell Plast 38:113–128

20. Yang CT, Lee ST (2003) Dimensional stability analysis of foams based on LDPE and ethylene–styrene interpolymer blends. J Cell Plast 39(1):59–69

21. Zhang H, Fang Z, Liu T, Li B, Li H, Cao Z, Jin G, Zhao L, Xin Z (2019) Dimensional stability of LDPE foams with CO_2 + i–C_4H_{10} mixtures as blowing agent: experimental and numerical simulation. Ind Eng Chem Res 58:13154–13162

22. Zhang H, Liu T, Li B, Li H, Cao Z, Jin G, Zhao L, Xin Z, (2020) Anti-shrinking foaming of polyethylene with CO_2 as blowing agent. J Supercrit Fluids 163.104883

23. Prissok F, Braun F, (2007) Foams based on thermoplastic polyurethanes. US9884947B2

24. Koshita N, Nishijima K, Oikawa M, Expanded thermoplastic polyurethane particles and expanded thermoplastic polyurethane particle molded article. US 20180155518 Al

25. Mix AW, Giacomin AJ (2011) Standardized polymer durometry. J Test Eval 39:1–10

26. Zhang R, Huang K, Hu S, Liu Q, Zhao X, Liu Y (2017) Improved cell morphology and reduced shrinkage ratio of ETPU beads by reactive blending. Polym Test 63:38–46

27. Wang W, Liao X, He Y, Li J, Jiang Q, Li G, (2020) Thermoplastic polyurethane/polytetrafluoroethylene composite foams with enhanced mechanical properties and anti-shrinkage capability fabricated with supercritical carbon dioxide. J Supercrit Fluids 163:104861

28. Wang W, Liao X, Guo F, Wang G, Yan Z, Liu F, Li G (2020) Facile fabrication of lightweight shape memory thermoplastic polyurethane/polylactide foams by supercritical carbon dioxide foaming. Ind Eng Chem Res 59:7611–7623

29. Zhao D, Wang G, Wang M (2018) Investigation of the effect of foaming process parameters on expanded thermoplastic polyurethane bead foams properties using response surface methodology. J Appl Polym Sci 135:46327

30. Lan B, Li P, Yang Q, Gong P, (2020) Dynamic self-generation of hydrogen bonding and relaxation of polymer chain segment in stabilizing thermoplastic polyurethane microcellular foams. Mater Today Commun 24:101056

31. Wang X, Mi J, Zhou H, Wang X (2018) Transition from microcellular to nanocellular chain extended poly (lactic acid)/hydroxyl-functionalized graphene foams by supercritical CO_2. J Mater Sci 54:3863–3877

32. Hossieny N, (2014) Development of expanded thermoplastic polyurethane bead foams and their sintering mechanism, Ph.D. Dissertation, Mechanical & Industrial Engineering Department, University of Toronto, Canada

33. Yeh SK, Yang J, Chiou NR, Daniel T, Lee LJ (2010) Introducing water as a co blowing agent in the carbon dioxide extrusion foaming process for polystyrene thermal insulation foams. Polym Eng Sci 50:1577–1584

34. Perez-Blanco M, Hammons JR, Danner RP (2010) Measurement of the solubility and diffusivity of blowing agents in polystyrene. J Appl Polym Sci 116:2359–2365

35. Huang SY (2018) Thermal properties of thermoplastic polyurethanes foam composed with different soft segments, MS Thesis. National Taiwan University of Science and Technology, Department of Materials Science and Engineering.

36. Lan B, Li P, Luo X, Luo H, Yang Q, Gong P, (2021) Hydrogen bonding and topological network effects on optimizing thermoplastic polyurethane/organic montmorillonite nanocomposite foam. Polymer 212:123159

37. Kumar V, Suh NP (1990) A process for making microcellular thermoplastic parts. Polym Eng Sci 30:1323–1329

38. Klempner D, Sendijarevic V, Aseeva RM (2004) Handbook of polymeric foams and foam technology. Hanser Verlag, Munich, Germany

39. Hayashi T, Koshita N, Oikawa M, (2019) Molded article of thermoplastic polyurethane foam particle sand method for manufacturing same and thermoplastic polyurethane foam particles. US20190153189A1

40. Furukawa M, Mitsui Y, Fukumaru T, Kojio K (2005) Microphase-separated structure and mechanical properties of novel polyurethane elastomers prepared with ether based diisocyanate. Polymer 46:10817–10822

41. Kojio K, Nakashima S, Furukawa M (2007) Microphase-separated structure and mechanical properties of norbornane diisocyanate-based polyurethanes. Polymer 48:997–1004

42. Kong Z, Tian Q, Zhang R, Yin J, Shi L, Ying WB, Hu H, Yao C, Wang K, Zhu J, (2019) Reexamination of the microphase separation in MDI and PTMG based polyurethane: Fast and continuous association/dissociation processes of hydrogen bonding. Polymer 185:121943

43. Hayashi T, Oikawa M, Koshita N, Thermoplastic polyurethane foaming particle and thermoplastic polyurethane foaming particle molded body. JP2018044042A

44. Keinath SE, Boyer RF (1981) Thermomechanical analysis of T_g and $T > T_g$ transitions in polystyrene. J Appl Polym Sci 26:2077–2085

45. Seymour RW, Cooper SL (1971) DSC studies of polyurethane block polymers. J Polym Sci Part B: Polymer Letters 9:689–694

46. Seymour RW, Cooper SL (1973) Thermal analysis of polyurethane block polymers. Macromolecules 6:48–53

47. Lamba NMK, Woodhouse KA, Cooper SL (1998) Polyurethanes in biomedical applications. CRC Press, Boca Raton, FL, USA

48. Chen TK, Chui JY, Shieh TS (1997) Glass transition behaviors of a polyurethane hard segment based on 4,4'-diisocyanatodiphenylmethane and 1,4-butanediol and the calculation of microdomain composition. Macromolecules 30:5068–5074

49. Abouzahr S, Wilkes GL, Ophir Z (1982) Structure-property behaviour of segmented polyether-MDI-butanediol based urethanes: effect of composition ratio. Polymer 23:1077–1086

50. Briscoe BJ, Savvas T, Kelly CT (1994) "Explosive decompression failure" of rubbers: A review of the origins of pneumatic stress induced rupture in elastomers. Rubber Chem Technol 67:384–416

51. Briscoe BJ, Zakaria S (1990) Gas-induced damage in elastomeric composites. J Mater Sci 25:3017–3023

52. Urbanczyk L, Calberg C, Detrembleur C, Jérôme C, Alexandre M (2010) Batch foaming of SAN/clay nanocomposites with scCO$_2$: A very tunable way of controlling the cellular morphology. Polymer 51:3520–3531

53. Bureau MN, Kumar V (2006) Fracture toughness of high-density polycarbonate microcellular foams. J Cell Plast 42:229–240

54. Seeler KA, Kumar V (1993) Tension-tension fatigue of microcellular polycarbonate: initial results. J Reinf Plast Compos 12:359–376

55. Zettl B, Mayer H, Stanzl-Tschegg SE, Degischer HP (2000) Fatigue properties of aluminium foams at high numbers of cycles. Mater Sci Eng A 292:1–7

56. Yeh SK, Huang CH, Su CC, Cheng KC, Chuang TH, Guo WJ, Wang SF (2013) Effect of dispersion method and process variables on the properties of supercritical CO$_2$ foamed polystyrene/graphite nanocomposite foam. Polym Eng Sci 53:2061–2072

57. Krause B, Sijbesma HJP, Munuklu P, van der Vegt NFA, Wessling M (2001) Bicontinuous nanoporous polymers by carbon dioxide foaming. Macromolecules 34:8792–8801

58. Li R, Lee JH, Wang C, Howe Mark L, Park CB, (2019) Solubility and diffusivity of CO$_2$ and N$_2$ in TPU and their effects on cell nucleation in batch foaming. J Supercrit Fluids 154:104623

59. Macosko CW (1994) Rheology principles, measurements, and applications. VCH, New York, NY, USA